American Mineralogist, Volume 84, pages 1135–1143, 1999

Symmetry change of majorite solid-solution in the system $Mg_3Al_2Si_3O_{12}$-$MgSiO_3$

AKIHIKO NAKATSUKA,[1,*] AKIRA YOSHIASA,[2] TAKAMITSU YAMANAKA,[2] OSAMU OHTAKA,[2] TOMOO KATSURA,[3] AND EIJI ITO[3]

[1]Department of Advanced Materials Science and Engineering, Faculty of Engineering, Yamaguchi University, Ube, Yamaguchi 755-8611, Japan
[2]Department of Earth and Space Science, Graduate School of Science, Osaka University, Toyonaka, Osaka 560-0043, Japan
[3]Institute for Study of the Earth's Interior, Okayama University, Misasa, Tottori 682-0193, Japan

ABSTRACT

Six single crystals of $Mg_3(Mg_xSi_xAl_{2-2x})Si_3O_{12}$ with x = 0.05, 0.13, 0.24, 0.38, 0.52, and 0.64 (the majorite solid-solution) were synthesized at 20 GPa and 2000 °C with a "6-8" type uniaxial split-sphere apparatus. Single-crystal X-ray diffraction studies revealed discontinuities in compositional dependence of the molar volume, equivalent isotropic temperature factors (B_{eq}), and mean bond lengths between x = 0.24 and 0.38. Single crystals in the compositional range $0 \le x \le 0.24$ show no birefringence, whereas those of x = 0.64 have a slight optical anisotropy. Moreover, the cell symmetry for x = 0.64 obtained using synchrotron X-ray radiation is tetragonal with a slight deviation from cubic. On the basis of site splitting expected from compositional dependence of B_{eq} obtained by cubic refinement, the most probable space group in the range $0.38 \le x \le 0.64$ is $I4_1/acd$ (tetragonal), which is the maximal subgroup of the space group $Ia\bar{3}d$ (cubic). Given that the previous reports that crystals with $0.8 \le x \le 1.0$ have the tetragonal space group $I4_1/a$, the majorite solid-solution in this system undergoes the series of symmetry changes, $Ia\bar{3}d \rightarrow I4_1/acd \rightarrow I4_1/a$, with increasing $MgSiO_3$ component. The symmetry changes from $Ia\bar{3}d$ to $I4_1/acd$ cannot be explained by the cation ordering on the octahedral site. Strong electrostatic interaction between the dodecahedral (Mg^{2+}) and tetrahedral (Si^{4+}) cations was observed from atomic thermal motion and electron density distribution. Because one of the site symmetries of the two nonequivalent tetrahedral sites in $I4_1/acd$ structure loses the center of symmetry with the symmetry reduction from $Ia\bar{3}d$ to $I4_1/acd$, the symmetry reduction may be caused by the electronic polarization of the cations due to the neighboring cation-cation interaction.

INTRODUCTION

Considerable efforts have been devoted to the investigations on crystal chemistry of garnets because of their importance in Earth's crust and in the upper mantle. A garnet phase called majorite is stable under pressure-temperature condition corresponding to the transition zone in Earth's mantle between the 400 and 670 km seismic discontinuities (e.g., Ringwood 1967; Liu 1977; Akaogi and Akimoto 1977; Ito and Takahashi 1987). Majorite in Earth's mantle is considered to be solid-solution having complex chemical composition of Mg-Ca-Fe-Cr-Al-Si-O system. As the simplest model, the chemical composition of majorite in Earth's mantle can be approximated by the solid-solution $Mg_3Al_2Si_3O_{12}$-$MgSiO_3$. The structure formula of this majorite solid-solution can be expressed as $Mg_3(Mg_xSi_xAl_{2-2x})Si_3O_{12}$. It has been reported that the cubic symmetry ($Ia\bar{3}d$) in this system is stable for $0 \le x < 0.8$, whereas that the symmetry in the range $0.8 \le x \le 1.0$ is tetragonal ($I4_1/a$) and the ordering of Mg^{2+} and Si^{4+} cations occurs on the two nonequivalent octahedral sites (e.g., Kato and Kumazawa 1985; Sawamoto 1987; Angel et al. 1989; Parise et al. 1996; Heinemann et al. 1997).

Angel et al. (1989) reported from transmission electron microscopic (TEM) observation that the two different types of merohedral and pseudomerohedral twins were invariably observed in $MgSiO_3$ majorite synthesized at 17 GPa and 1800 °C. They argued that Mg-Si ordering process is unlikely to be completed within only a few seconds during the quenching and these twins will arise during crystal growth; and thus, that $MgSiO_3$ majorite is tetragonal ($I4_1/a$) under high pressure-temperature condition corresponding to the transition zone in Earth's mantle. However, from the symmetry analysis based on group theory, Hatch and Ghose (1989) interpreted the observed twinning in $MgSiO_3$ majorite as evidence of a phase transition from $Ia\bar{3}d$ to $I4_1/a$ caused during the quenching, and argued that $MgSiO_3$ majorite in the transition zone is cubic with complete Mg-Si disordering on octahedral site. Wang et al. (1993) concluded from the synthetic temperature dependence of microstructures that the phase transition from $Ia\bar{3}d$ to $I4_1/a$ in $MgSiO_3$ majorite arises around 22 GPa and 2300–2350 °C and that the ubiquitous twins in $I4_1/a$ phase synthesized below this temperature are produced during the growth process. Consequently, they considered that $MgSiO_3$ majorite in the transition zone is probably tetragonal ($I4_1/a$). Recently, in $Mg_3Al_2Si_3O_{12}$-$MgSiO_3$ majorite solide solution, Heinemann et al. (1997) proposed that the phase transition of the end-mem-

*E-mail: tuka@po.cc.yamaguchi-u.ac.jp

ber $MgSiO_3$ majorite from high-temperature phase ($Ia\bar{3}d$) to low-temperature phase ($I4_1/a$) occurs at 19 GPa and 1500 °C and the boundary between the both phases shifts to low temperature side with increasing $Mg_3Al_2Si_3O_{12}$ component. As a result, they argued that the majorite solid-solution has cubic symmetry ($Ia\bar{3}d$) through the whole compositions under the condition of the transition zone in Earth's mantle. Thus, there is some disagreement about the actual symmetry at the pressure-temperature conditions of the transition zone in Earth's mantle. Moreover, an intermediate tetragonal phase ($I4_1/acd$) has been suggested from the coexistence of pseudomerohedral and merohedral twins in the end-member $MgSiO_3$ majorite (e.g., Wang et al. 1993), because the former results from the symmetry change from $Ia\bar{3}d$ to $I4_1/acd$ and the latter is related to that from $I4_1/acd$ to $I4_1/a$. However, Heinemann et al. (1997) considered the existence of $I4_1/acd$ phase in the majorite solid-solution unlikely.

In this paper, single-crystal X-ray diffraction study of the majorite solid-solution in the system $Mg_3Al_2Si_3O_{12}$-$MgSiO_3$ is carried out systematically to gain information on the crystal chemical relation between the cubic and tetragonal phases. A new lower symmetric garnet phase is found for compositions previously considered to be cubic. The reason for the symmetry change from cubic phase to the new lower symmetric phase is discussed from a viewpoint of crystal chemistry, with attention to the electrostatic neighboring cation-cation interaction connected with our previous studies (Nakatsuka et al. 1995 and Yoshiasa et al. 1997).

Experimental details and structure refinements

Six single crystals of majorite solid-solution in the system $Mg_3Al_2Si_3O_{12}$-$MgSiO_3$ were synthesized under high-pressure and high-temperature (20 GPa and 2000 °C) using a 1000 and 5000 ton "6-8" type uniaxial split-sphere apparatus (USSA-1000 and 5000) installed at the ISEI of Okayama University. All specimens were synthesized from the same starting materials and under the same pressure-temperature condition. Special grade reagents (99.99%) of MgO, Al_2O_3, and SiO_2 were used as starting materials. These oxides were mixed together in appropriate molar ratios. A 15 mol% flux of PbO was mixed with the starting materials. The anvil assembly of tungsten carbide cubes with a truncated edge length of 5 mm was compressed with the aid of USSA-1000 and 5000. A 10 mm regular octahedron of a sintered MgO containing 5% of Cr_2O_3 was used as pressure medium. The powder mixtures were put into a cylindrical rhenium heater embedded in the MgO octahedron. Because MgO has a high thermal conductivity, an $LaCrO_3$ sleeve was inserted outside of the rhenium heater. The sample temperature was monitored by the W25%Re-W3%Re thermocouple with 0.05 mm in diameter. The junction of the thermocouple was put at the midpoint of the outer surface of the cylindrical rhenium heater. No correction was made for the pressure effect on emf. After being kept at the desired condition (20 GPa and 2000 °C) for 1 hour, the product was quenched by shutting off the electric power supply. The pressure was released slowly and the products were recovered at ambient conditions. Compositions of the single crystals (Table 1) were determined by means of a JEOL JCMA-733II electron microprobe analyzer (EPMA). No contamination of Pb into the single crystals was detected from qualitative analyses by EPMA.

Unit-cell parameters and diffraction intensity data were measured at room temperature using a four circle diffractometer (Rigaku AFC-5S) operated at 45 kV and 40 mA. The graphite-monochromatized Mo$K\alpha$ (λ = 0.71069 Å) radiation was used for the measurements. The unit-cell parameters of each specimen were determined by the least-squares method from a set of 25 reflections within the range of $40° \le 2\theta \le 50°$. Prior to the measurements, zero-point adjustment for the four circle diffractometer was carried out. The zero-point correction angles were $\Delta 2\theta = 0.000°$, $\Delta\omega = -0.030°$, $\Delta\chi = 0.000°$, and $\Delta\phi = 0.000°$, and the four circle diffractometer used were adjusted very well. The unit-cell parameter of the single-crystal silicon standard was a_0 = 5.4312(3) Å, which agrees very well with the JCPDS value (a_0 = 5.43088 Å). This agreement indicates that the unit-cell parameters of majorite solid-solution obtained in the present study are reliable. Intensity data within $(\sin\theta)/\lambda \le 0.807$ with $0 \le h, k, l \le 18$ were collected by continuous ω scan mode. Lorentz and polarization corrections were applied, whereas no correction was made for absorption effect because the linear absorption coefficients (μ) for each specimen were sufficiently small (Table 2). The nearly constant transmission was observed in ψ scan for the selected reflections even the specimen x = 0.24 having the greatest aspect ratio of the specimens investigated, showing that the influence of the crystal aspect on absorption effect is negligible. Reflections between 1875 and 1892 were measured for each specimen. The observed reflections with $|F_o| \ge 3\sigma(|F_o|)$ varied between 595 and 1051 for the different structure refinements. The unit-cell parameter of the specimen with x = 0.64 was also measured using synchrotron X-ray radiation, which yields higher 2θ resolution, with the four circle diffractometer installed at BL-10A in the Photon Factory of the National Laboratory for High Energy Physics. The synchrotron X-ray radiation of wavelength λ = 1.000 Å was obtained from the 2.5 GeV storage ring using a Si(111) double-crystal monochromator. The unit-cell parameter of the specimen x = 0.64 obtained using the synchrotron X-ray radiation was determined by the least-squares method from the same set of 25 reflections as that adopted for the measurements using conventional X-ray source.

The crystal-structure refinements were carried out by minimizing the function $\Sigma w(|F_o| - |F_c|)^2$ using a full matrix least-squares program RFINE2 (Finger 1969). As will be described below, the specimens with x = 0.38, 0.52, and 0.64 exhibit the possibility of tetragonal symmetry ($I4_1/acd$). The structure refinements were, therefore, performed by assuming two space groups $Ia\bar{3}d$ and $I4_1/acd$. As the first step, the crystal structures of all specimens were refined in the space group $Ia\bar{3}d$. As the second step, the space group $I4_1/acd$ was assumed in the structure refinements for the specimens of x = 0.38, 0.52, and 0.64. Atomic scattering factors for neutral atoms and anomalous dispersion coefficients were taken from *International Tables for X-ray Crystallography* (Ibers and Hamilton 1974). The occupancy parameters were not refined because of similar atomic scattering curves of Mg, Al, and Si atoms. In consideration of cation distribution expected from cation sizes (Shannon 1976),

TABLE 1. Results of chemical analyses by electron microprobe analyzer

	x = 0.0.5(1)		x = 0.13(1)		x = 0.24(1)		x = 0.38(1)		x = 0.52(1)		x = 0.64(1)	
Element	wt%	Cation ratio	wt%	Cation ratio	wt%	Cation ratio	wt%	Cation ratio	wt%	Cation ratio	wt%	Cation ratio
MgO	30.78(16)	3.05(1)	30.69(16)	3.12(1)	32.02(16)	3.23(1)	34.00(16)	3.38(1)	34.94(17)	3.52(1)	36.37(17)	3.63(1)
SiO_2	45.78(19)	3.05(1)	45.92(19)	3.13(1)	47.91(19)	3.24(1)	50.57(20)	3.38(1)	52.08(20)	3.52(1)	54.38(20)	3.64(1)
Al_2O_3	24.29(14)	1.90(1)	21.61(13)	1.74(1)	19.10(12)	1.52(1)	15.43(11)	1.22(1)	12.06(10)	0.96(1)	8.14(8)	0.64(1)
Total	100.85	8.00	98.22	7.99	99.03	7.99	100.00	7.98	99.08	8.00	98.89	7.91

TABLE 2a. Crystallographic data and data-collection and refinement parameters of cubic garnets

Composition	x = 0.05	x = 0.13	x = 0.24
a_0(Å)	11.4666(10)	11.4755(9)	11.4915(8)
V(Å^3)	1507.7(4)	1511.2(4)	1517.5(3)
Space group assumed	$Ia\bar{3}d$	$Ia\bar{3}d$	$Ia\bar{3}d$
Density (g/cm^3)	3.553	3.543	3.527
Radiation used	Mo$K\alpha$	Mo$K\alpha$	Mo$K\alpha$
Monochromator	graphite	graphite	graphite
Crystal size (mm)	$0.14 \times 0.14 \times 0.12$	$0.06 \times 0.06 \times 0.05$	$0.13 \times 0.07 \times 0.06$
μ (cm^{-1})	12.10	12.07	12.02
Scan type	ω	ω	ω
Scan speed (°/min)	4	1	2
2θ range (°)	$2 \le 2\theta \le 70$	$2 \le 2\theta \le 70$	$2 \le 2\theta \le 70$
Range of h,k,l	$0 \le h,k,l \le 18$	$0 \le h,k,l \le 18$	$0 \le h,k,l \le 18$
Measured reflections	1875	1877	1892
Observed reflections with $\lvert F_o\rvert \ge 3\sigma(\lvert F_o\rvert)$	1051	711	896
No. of parameters	18	18	18
Scale factor	0.380(7)	0.082(2)	0.13(1)
Extinction coefficient	$0.13(1) \times 10^{-7}$	$0.37(8) \times 10^{-8}$	$0.51(7) \times 10^{-8}$
R (%)	2.33	2.59	2.68
R_w (%)	1.97	1.86	2.09
Weighting scheme	$1/\sigma^2(\lvert F_o\rvert)$	$1/\sigma^2(\lvert F_o\rvert)$	$1/\sigma^2(\lvert F_o\rvert)$

TABLE 2b. Parameters for potentially non-cubic garnets

Composition	x = 0.38	x = 0.52	x = 0.64
a_0(Å) (pseudocubic cell)	11.4833(11)	11.4876(8)	11.4891(8)
V(Å^3)	1514.3(4)	1516.0(3)	1516.6(3)
Space group assumed	$I4_1/acd$	$I4_1/acd$	$I4_1/acd$
Density (g/cm^3)	3.533	3.527	3.524
Radiation used	Mo$K\alpha$	Mo$K\alpha$	Mo$K\alpha$
Monochromator	graphite	graphite	graphite
Crystal size (mm)	$0.12 \times 0.10 \times 0.07$	$0.10 \times 0.10 \times 0.06$	$0.12 \times 0.07 \times 0.06$
μ (cm^{-1})	12.05	12.04	12.04
Scan type	ω	ω	ω
Scan speed (°/min)	2	2	2
2θ range (°)	$2 \le 2\theta \le 70$	$2 \le 2\theta \le 70$	$2 \le 2\theta \le 70$
Range of h,k,l	$0 \le h,k,l \le 18$	$0 \le h,k,l \le 18$	$0 \le h,k,l \le 18$
Measured reflections	1892	1892	1877
Observed reflections with $\lvert F_o\rvert \ge 3\sigma(\lvert F_o\rvert)$	1033	766	595
	cubic ($Ia\bar{3}d$) refinements		
No. of parameters	18	18	18
Scale factor	0.18(1)	0.11(1)	0.17(1)
Extinction coefficient	$0.38(7) \times 10^{-8}$	$0.47(8) \times 10^{-8}$	$0.64(10) \times 10^{-8}$
R (%)	2.62	2.92	2.91
R_w (%)	2.27	2.17	1.95
Weighting scheme	$1/\sigma^2(\lvert F_o\rvert)$	$1/\sigma^2(\lvert F_o\rvert)$	$1/\sigma^2(\lvert F_o\rvert)$
	tetragonal ($I4_1/acd$) refinements		
No. of parameters	50	50	50
Scale factor	0.18(1)	0.11(1)	0.17(1)
Extinction coefficient	$0.36(7) \times 10^{-8}$	$0.47(8) \times 10^{-8}$	$0.64(10) \times 10^{-8}$
R (%)	2.61	2.88	2.83
R_w (%)	2.23	2.13	1.92
Weighting scheme	$1/\sigma^2(\lvert F_o\rvert)$	$1/\sigma^2(\lvert F_o\rvert)$	$1/\sigma^2(\lvert F_o\rvert)$

TABLE 3. Refined positional parameters and equivalent isotropic temperature factors (Å²), and fixed occupancy parameters in $Ia\bar{3}d$ (cubic) refinements

Octahedral Si	Site	*x*	*y*	*z*	B_{eq}*	Occupancy parameters		
						Mg^{2+}	Si^{4+}	Al^{3+}
0.05	X	0.125	0	0.25	0.86(1)			
	Y	0	0	0	0.38(1)	0.025	0.025	0.950
	Z	0.375	0	0.25	0.36(1)			
	O	–0.03278(5)	0.05012(6)	0.15345(6)	0.52(1)			
0.13	X				0.89(1)			
	Y				0.37(1)	0.065	0.065	0.870
	Z				0.41(1)			
	O	–0.03275(7)	0.05012(7)	0.15370(7)	0.58(1)			
0.24	X				0.80(1)			
	Y				0.48(1)	0.119	0.119	0.762
	Z				0.50(1)			
	O	–0.03306(7)	0.05050(7)	0.15407(7)	0.72(1)			
0.38	X				1.21(1)			
	Y				0.26(1)	0.187	0.187	0.626
	Z				0.50(1)			
	O	–0.03278(6)	0.05022(7)	0.15422(7)	0.82(1)			
0.52	X				1.07(1)			
	Y				0.47(1)	0.260	0.260	0.480
	Z				0.53(1)			
	O	–0.03281(8)	0.05034(8)	0.15414(8)	0.86(1)			
0.64	X				1.46(1)			
	Y				0.33(1)	0.320	0.320	0.360
	Z				0.58(1)			
	O	–0.03246(10)	0.05031(10)	0.15459(10)	1.02(1)			

Notes: X = dodecahedral site; Y = octahedral site; Z = tetrahedral site; O = oxygen site.
* $B_{eq} = (4/3)\Sigma_i\Sigma_j\beta_{ij}\mathbf{a}_i.\mathbf{a}_j$.

TABLE 4. Refined positional parameters and equivalent isotropic temperature factors (Å²), and fixed occupancy parameters in $I4_1/acd$ (tetragonal) refinements

Octahedral Si	Site	*x*	*y*	*z*	B_{eq}*	Occupancy parameters		
						Mg^{2+}	Si^{4+}	Al^{3+}
0.38	X1	0	0.25	0.125	1.21(2)			
	X2	0.12495(10)	0	0.25	1.21(2)			
	Y	0	0	0	0.26(1)	0.187	0.187	0.626
	Z1	0	0.25	0.375	0.50(1)			
	Z2	0.37505(7)	0	0.25	0.51(1)			
	O1	–0.03273(12)	0.05009(12)	0.15398(12)	0.81(2)			
	O2	0.15438(12)	–0.03268(12)	0.05053(11)	0.83(2)			
	O3	0.05005(12)	0.15430(12)	–0.03292(11)	0.82(2)			
0.52	X1				1.07(2)			
	X2	0.12502(12)	0	0.25	1.06(2)			
	Y				0.47(1)	0.260	0.260	0.480
	Z1				0.54(1)			
	Z2	0.37505(9)	0	0.25	0.52(1)			
	O1	–0.03272(15)	0.05022(16)	0.15410(14)	0.84(2)			
	O2	0.15435(15)	–0.03282(15)	0.05052(14)	0.89(2)			
	O3	0.05029(15)	0.15399(14)	–0.03288(13)	0.83(2)			
0.64	X1				1.48(2)			
	X2	0.12494(19)	0	0.25	1.46(2)			
	Y				0.33(1)	0.320	0.320	0.360
	Z1				0.57(1)			
	Z2	0.37500(14)	0	0.25	0.59(1)			
	O1	–0.03240(19)	0.05055(20)	0.15462(17)	1.04(2)			
	O2	0.15446(19)	–0.03260(18)	0.05013(16)	1.03(2)			
	O3	0.05023(19)	0.15470(18)	–0.03237(16)	0.99(2)			

Notes: X1, X2 =dodecahedral sites; Y = octahedral site; Z1, Z2 = tetrahedral sites; O1, O2, O3 = oxygen sites.
* $B_{eq} = (4/3)\Sigma_i\Sigma_j\beta_{ij}\mathbf{a}_i.\mathbf{a}_j$.

the cation ratios calculated from the results of chemical analyses (Table 1) indicate that in the both cases of $Ia\bar{3}d$ and $I4_1/acd$ structures the substitution of the cations, $2Al^{3+} \leftrightarrow Mg^{2+} + Si^{4+}$, occurs only on one equivalent octahedral site. Therefore, the occupancy parameters for each site were fixed based on the results of chemical analyses. During the least-squares refinements, the correction for isotropic extinction effect was made. After several cycles of refinements, temperature factors were converted to the anisotropic model. The crystallographic data and data-collection and refinement parameters are given in Table 2. The structure parameters obtained by cubic and tetragonal refinements are listed in Tables 3 and 4, respectively.

RESULTS AND DISCUSSION

Symmetry change

Figure 1 shows a variation of molar volumes against composition (x). Two discontinuities are observed in Figure 1. The discontinuity observed in the compositional range between x = 0.64 and 1.0 is due to the previously reported symmetry change from $Ia\bar{3}d$ to $I4_1/a$ (e.g., Kato and Kumazawa 1985; Sawamoto 1987; Angel et al. 1989; Heinemann et al. 1997). Here, another discontinuity is newly observed between x = 0.24 and 0.38 in Figure 1. From the polarization-microscopic studies, the single crystals in the range $0 \le x \le 0.24$ exhibit no birefringence, whereas the single crystals with x = 0.64 exhibit slight birefringence, and it is difficult to observe birefringence of those of x = 0.38 and 0.52. Retardation of the specimen x = 0.64 with the thickness of about 200 μm was the same degree as that of quartz with the thickness of 20 μm estimated from Michel-Lévy's interference color chart. Thus, the value of the birefringence for the specimen x = 0.64 is below 0.001. The single crystals of x = 0.64 show "normal," not undulatory, extinction under crossed polars. This strongly suggests that the appearance of the birefringence in the specimen x = 0.64 is due to not ferroelastic strain but to symmetry reduction from cubic. Therefore, from Figure 1 and the polarization-microscopic observations, we conclude that majorite solid-solution in the range $0 \le x \le 0.24$ has cubic symmetry, while that in the range $0.38 \le x \le 0.64$, which was previously assigned to cubic phase, has a lower symmetry than cubic.

Although the unit-cell parameters of three specimens in the range $0.38 \le x \le 0.64$ measured using conventional X-ray source indicate pseudocubic cell (Table 2), the unit-cell parameter of x = 0.64 using synchrotron X-ray radiation has the dimensions a = 11.541(1) Å, b = 11.542(1) Å, and c = 11.532(1) Å with interaxial angles statistically equal to 90°. This clearly exhibits a tetragonal unit cell. The discrepancy between the cell symmetries obtained by conventional and synchrotron X-ray radiation sources is due to the difference in 2θ resolution. Hence, the cell symmetry obtained by synchrotron X-ray radiation is more reliable. Possible tetragonal space groups should be subgroups of $Ia\bar{3}d$ that allow the garnet structure to be maintained, and the candidates are $I4_1/acd$ and $I4_1/a$ (e.g., Takéuchi et al. 1982). The space group $I4_1/acd$ is the maximal subgroup of $Ia\bar{3}d$, and $I4_1/a$ is that of $I4_1/acd$. The symmetry changes from $Ia\bar{3}d$ to $I4_1/acd$ and from $I4_1/acd$ to $I4_1/a$ yield the split of sites as shown in Table 5.

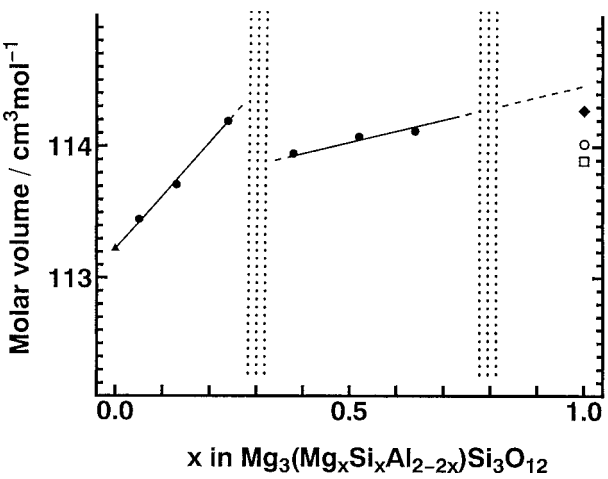

FIGURE 1. Compositional dependence of molar volume in majorite solid-solution. Solid circle = this study; solid triangle = Novak and Gibbs (1971); solid diamond = Angel et al. (1989); open circle = Heinemann et al. (1997); open square = Sinogeikin et al. (1997). Solid circle, solid triangle, and solid diamond are data from the single crystals; open circle and open square are data from the powder crystals.

The equivalent isotropic temperature factors (B_{eq}) refined by X-ray diffraction represent the atomic positional disorder together with thermal vibrations of atoms. If the symmetry is reduced from cubic to the lower symmetry, the apparent B_{eq} values obtained by structural refinement based on cubic symmetry ($Ia\bar{3}d$) should be estimated to be larger than those from refinement based on the lower symmetry. Figure 2 shows a discontinuity between x = 0.24 and 0.38 where the symmetry reduction described above occurs. Upon symmetry reduction, the B_{eq} values of the dodecahedral, tetrahedral, and oxygen atoms in the range $0.38 \le x \le 0.64$ become larger than those in the range $0 \le x \le 0.24$, whereas the B_{eq} value of the octahedral cation in the range $0.38 \le x \le 0.64$ becomes smaller than that in the range 0

TABLE 5. Occupied sites in garnet structures

Site	Wyckoff position	Site symmetry	Atomic coordinates
		Ia$\bar{3}$d	
X	24c	222	1/8, 0, 1/4
Y	16a	$\bar{3}$	0, 0, 0
Z	24d	$\bar{4}$	3/8, 0, 1/4
O	96h	1	*x, y, z*
		I4$_1$/acd	
X1	8b	222	0, 1/4, 1/8
X2	16e	2	*x*, 0, 1/4
Y	16c	$\bar{1}$	0, 0, 0
Z1	8a	$\bar{4}$	0, 1/4, 3/8
Z2	16e	2	*x*, 0, 1/4
O1	32g	1	*x, y, z*
O2	32g	1	*x, y, z*
O3	32g	1	*x, y, z*
		I4$_1$/a	
X1	16f	1	*x, y, z*
X2	8e	2	–1/2, 1/4, *z*
Y1	8c	$\bar{1}$	–1/2, 0, 1/2
Y2	8d	$\bar{1}$	–1/2, 0, 0
Z1	4a	$\bar{4}$	–1/2, 1/4, 3/8
Z2	4b	$\bar{4}$	–1/2, 1/4, 7/8
Z3	16f	1	*x, y, z*
O1	16f	1	*x, y, z*
O2	16f	1	*x, y, z*
O3	16f	1	*x, y, z*
O4	16f	1	*x, y, z*
O5	16f	1	*x, y, z*
O6	16f	1	*x, y, z*

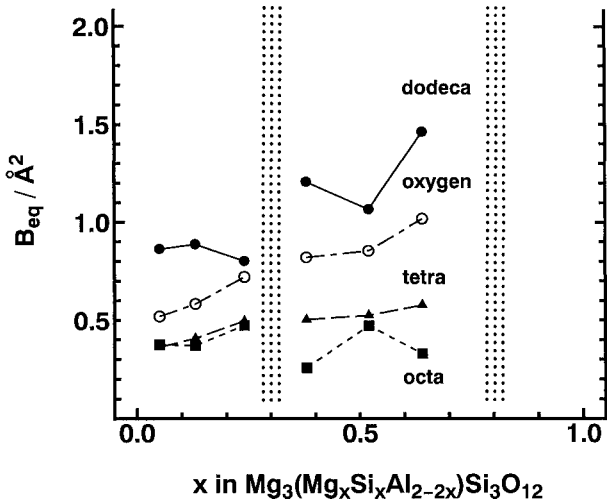

FIGURE 2. Compositional dependence of equivalent isotropic temperature factors (B_{eq}) of majorite solid-solution in cubic refinements. Solid circle = dodecahedral cation; solid square = octahedral cation; solid triangle = tetrahedral cation; open circle = oxygen.

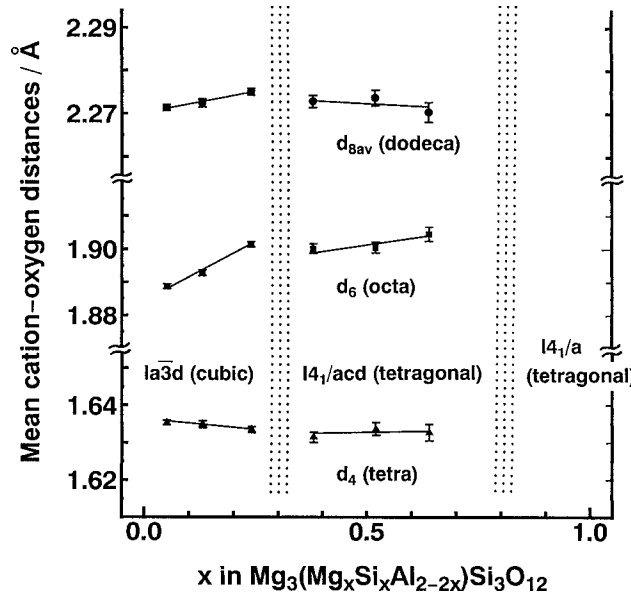

FIGURE 3. Compositional dependence of the mean cation-oxygen distances in majorite solid-solution. Solid circle = dodecahedral site (d_{8av}); solid square = octahedral site (d_6); solid triangle = tetrahedral site (d_4). The average values of the nonequivalent cation-oxygen distances in $I4_1/acd$ structure regarded as the equivalent ones in $Ia\bar{3}d$ structure are plotted for $I4_1/acd$ phase in the Figure.

$\leq x \leq 0.24$. This difference suggests that the dodecahedral, tetrahedral, and oxygen sites separate into more than two sites with symmetry reduction observed in the range $0.24 < x < 0.38$, but that the octahedral site does not separate. Only the space group $I4_1/acd$ among subgroups of $Ia\bar{3}d$ satisfies these relationships, and is therefore considered to be the most likely space group in the range $0.38 \leq x \leq 0.64$. Consequently, the majorite solid-solution in the system $Mg_3Al_2Si_3O_{12}$-$MgSiO_3$ undergoes the following series of symmetry changes with increasing $MgSiO_3$ component: $Ia\bar{3}d \rightarrow I4_1/acd \rightarrow I4_1/a$. The discontinuity in the mean bond lengths is also observed in the range $0.24 < x < 0.38$ (Fig. 3). The gap observed on the octahedral site between $Ia\bar{3}d$ and $I4_1/acd$ phases is greatest among all bond lengths. The structure refinements for $x = 0.38$, 0.52, and 0.64 based on the space group $I4_1/acd$ (tetragonal) resulted in very small deviation from cubic ($Ia\bar{3}d$) (Tables 3 and 4), and *R*-values obtained from $I4_1/acd$ refinements were not improved significantly compared with those from the cubic refinements (Table 2b). In addition, the B_{eq} values from the refinements based on $I4_1/acd$ for $x = 0.38$, 0.52, and 0.64 are little different from those assuming $Ia\bar{3}d$ (Tables 3 and 4). This may be due to a limitation of the resolution for the split of dodecahedral, tetrahedral, and oxygen sites because of the small deviation from cubic symmetry. The same situation was also seen in the birefringent silicate garnet having $I4_1/acd$ symmetry reported by Griffen et al. (1992).

Except for one case wherein additional Jahn-Teller distortion was indicated, the symmetry reduction for all lower symmetric garnets reported by previous studies (e.g., Takéuchi et al. 1982; Kato and Kumazawa 1985; Fujino et al. 1986; Sawamoto 1987; Angel et al. 1989; Griffen et al. 1992; Hazen et al. 1994) has been attributed to cation ordering on nonequivalent octahedral and/or dodecahedral sites connected with the difference between cation sizes on mixing sites. However, this is not the case for the majorite solid-solution in $I4_1/acd$ phase($0.38 \leq x \leq 0.64$) because the substitution of cations, $2Al^{3+} \leftrightarrow Mg^{2+} + Si^{4+}$, occurs only on one equivalent octahedral site in the $I4_1/acd$ structure. Thus, cation ordering in garnet structure is not the direct reason for the symmetry reduction from cubic, and other factors need to be considered as the driving force.

Cation-cation interaction and residual electron density distribution

The repulsive force between the dodecahedral (Mg^{2+}) and tetrahedral (Si^{4+}) cations across the shared edge (d_{48}) is expected to be strong because the Mg-Si distances of 2.867–2.873 Å for each specimen are shorter than those of other garnets (see Nakatsuka et al. (1995) for the nomenclature of the interatomic distances d_i). Thermal vibrations of dodecahedral (Mg^{2+}) and tetrahedral (Si^{4+}) cations (Fig. 4) are significantly smaller in the direction perpendicular to d_{48} than those in other directions, which indicates that the thermal vibrations are restrained between dodecahedral (Mg^{2+}) and tetrahedral (Si^{4+}) cations because of the strong repulsive force between the cations. Consequently, to shield this strong repulsive force, the shared edges d_{48} (2.475–2.495 Å for each specimen) are considerably shorter than $2r_o$ (2.76 Å), where r_o is ionic radius of oxygen (Shannon 1976). Such a shielding effect is revealed in the electron density distribution. In the difference Fourier map (Fig. 5), the maxima of the two positive residual peaks with height of 0.9 eÅ^{-3} in the field between dodecahedral (Mg^{2+}) and tetrahedral (Si^{4+}) cations are clearly observed at distance of 1.39 Å from the dodecahedral cation (Mg^{2+}). A "bridge" of electron density is formed by the connection of these residual peaks.

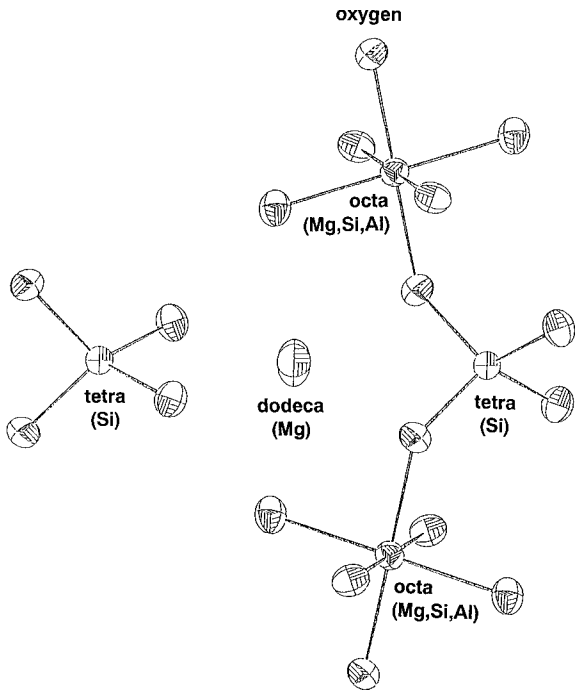

FIGURE 4. Thermal motion of dodecahedral, octahedral, tetrahedral, and oxygen atoms in the specimen $x = 0.05$ projected on (010). Atoms are drawn as ellipsoids of 99% probability (ORTEP, Johnson 1965).

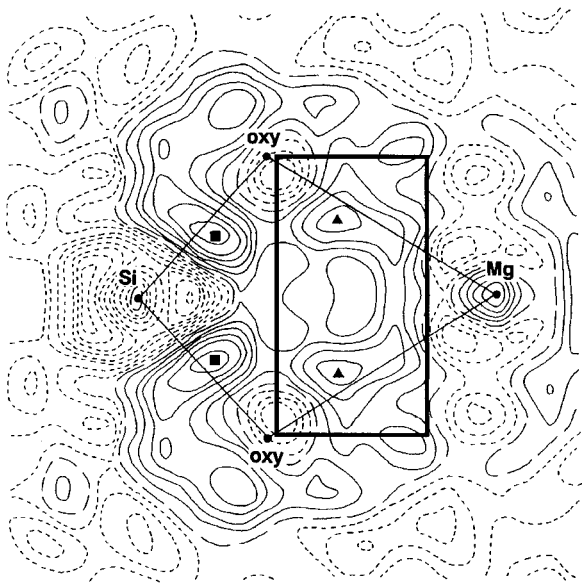

FIGURE 5. The section of the difference Fourier map on the plane which contains the two O atoms forming shared edge (d_{48}) and tetrahedral (Si) and dodecahedral (Mg) cations in the specimens $x = 0.05$. Small solid circles represent the atomic positions. The contour interval is 0.2 eÅ^{-3}. Positive contours are solid lines. Negative and zero contours are short and long dashed lines, respectively. The part surrounded by the rectangular frame shows the "bridge" of electron density. Solid triangle is the maxima of positive residual peaks forming the "bridge." Solid square represents the maxima of positive residual peaks corresponding to the bonding electrons on Si-O bonds.

The formation of the bridge is energetically favorable owing to the relaxation of the strong electrostatic repulsive force between dodecahedral (Mg^{2+}) and tetrahedral (Si^{4+}) cations. Hence, the shielding effect will be accomplished by the formation of the bridge.

Mg-O (d_8), Mg-O (d_{80}), (Mg, Si, Al)-O (d_6), and Si-O (d_4) bonds of the specimen $x = 0.05$ have covalencies of 18.3, 23.0, 35.7, and 53.5% respectively, according to the formulation of Brown and Shannon (1973). Because the Si-O bond is more covalent than the remaining bonds, the atomic orbitals of Si contribute more greatly to the formation of molecular orbitals forming the bridge than those of Mg. We now consider how a superposition of molecular orbitals formed mainly by interactions between atomic orbitals of Si and O atoms could produce the residual peaks forming the bridge. Molecular orbital calculations for the SiO_4^{4-} cluster using the DV-Xα method have been carried out by Adachi (1991). The "orbital populations" for each valence level, which are the proportion of the atomic orbital components included in the molecular orbitals, are listed in Table 6. The $4a_1$, $3t_2$, $5a_1$, and $4t_2$ orbitals are considered to be the bonding orbital formed by interaction between atomic orbitals of Si and O atoms, whereas the 1e, $5t_2$, and $1t_1$ orbitals are considered to be nonbonding molecular orbitals that are essentially contributed only by 2p(O) orbitals, although 1e and $5t_2$ orbitals have a slight contribution of 3d(Si) orbitals. In particular the $1t_1$ orbital corresponding to the highest occupied molecular orbital, is a nonbonding molecular orbital contributed only by 2p(O) orbitals without any contribution from other atomic orbitals. Because the maxima of residual peaks forming the bridge are not on the Si-O bond as seen in Figure 5 and will hardly contribute to the formation of the bond, origin of the bridge of electron density observed in the field between tetrahedral and dodecahedral cations is considered to be a superposition of nonbonding molecular orbitals formed essentially by 2p(O) orbitals, i.e., 1e, $5t_2$, and $1t_1$ orbitals. Thus, the strong electrostatic neighboring cation-cation interaction obviously exists in majorite solid-solution as seen in the atomic thermal motion (Fig. 4) and is relaxed by contact between 2p orbitals of O atoms forming the polyhedral shared edges.

A large positive residual electron density with height of 1.4 eÅ^{-3} is clearly observed at the center of Si-O bonds (d_4) in Figure 5. The electrons could be provided from the bonding molecular orbitals $4a_1$, $3t_2$, $5a_1$, and $4t_2$ in Table 6. The existence of this bonding electrons means that Si-O bond is rigid because of the strong covalency as seen in many silicates; this is consistent with a nearly constant Si-O distances vs. composition in Figure 3.

TABLE 6. Orbital populations for each valence level of SiO_4^{4-} cluster (%)*

	Molecular orbitals						
Atomic orbitals	$4a_1$	$3t_2$	$5a_1$	$4t_2$	1e	$5t_2$	$1t_1$
3s(Si)	8	–	13	–	–	–	–
3p(Si)	–	4	–	11	–	0	–
3d(Si)	–	2	–	0	5	5	–
2s(O)	86	93	11	3	–	0	–
2p(O)	5	1	76	87	95	94	100

* After Adachi 1991.

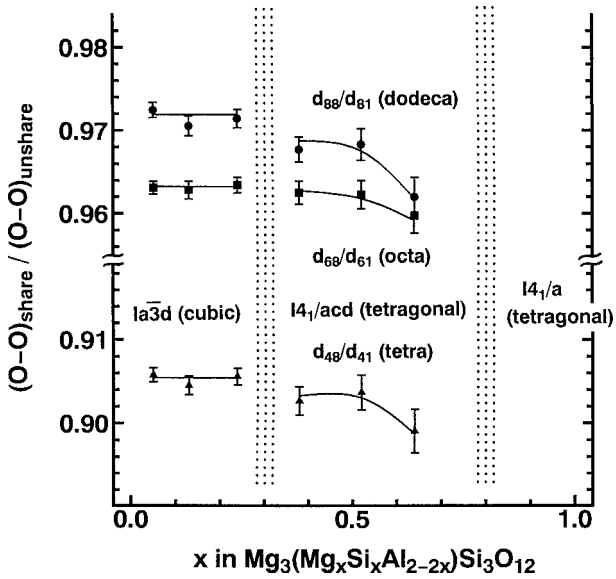

FIGURE 6. Compositional dependence of the ratio of the shared to the unshared O-O distances in each polyhedron in majorite solid-solution. Solid circle = dodecahedral site (d_{88}/d_{81}); solid square = octahedral site (d_{68}/d_{61}); solid triangle = tetrahedral site (d_{48}/d_{41}). The ratios $(O\text{-}O)_{shared}/(O\text{-}O)_{unshared}$ in $I4_1/acd$ structure are calculated from the averaged values of nonequivalent $(O\text{-}O)_{shared}$ distances and those of nonequivalent $(O\text{-}O)_{unshared}$ distances in $I4_1/acd$ structure regarded as the equivalent ones in $Ia\bar{3}d$ structure. The ratio $(O\text{-}O)_{shared}/(O\text{-}O)_{unshared}$ in dodecahedron is plotted by the ratio of the edge length (d_{88}) shared with different dodecahedron to the shortest length (d_{81}) of the three symmetrically nonequivalent unshared edges (d_{81}, d_{82}, and d_{83}) in $Ia\bar{3}d$ structure.

Effect of the neighboring cation-cation interaction on symmetry change

The ratio of the shared to unshared O-O distances has different dependences on composition for the cubic ($Ia\bar{3}d$) and tetragonal phases ($I4_1/acd$) (Fig. 6). The ratios d_{88}/d_{81}, d_{68}/d_{61}, and d_{48}/d_{41} in $Ia\bar{3}d$ phase are nearly constant, whereas those in $I4_1/acd$ phase are slightly lower and decrease with increasing $MgSiO_3$ component (i.e., with increasing the octahedral volume). As described by Nakatsuka et al. (1995), the increase in octahedral volume in cubic garnet ($Ia\bar{3}d$) should force the values of $(O\text{-}O)_{shared}/(O\text{-}O)_{unshared}$ for each polyhedron to increase from the structural geometric restriction and consequently result in the lessening of the shielding effect. However, it is energetically unfavorable for the majorite solid-solution with $Ia\bar{3}d$ structure to weaken the shielding effect, because the cation-cation interaction is originally great as described above. These competing effects give a nearly constant ratio for the $Ia\bar{3}d$ phase. This constant ratio suggests the acceptable limitation for the lessening of the shielding effect (i.e., for energetic stability of the crystal structure).To avoid such strong cation-cation interaction, the molar volume in $Ia\bar{3}d$ phase increases more dramatically with increasing $MgSiO_3$ component than that in the $I4_1/acd$ phase (Fig. 1). [The variation of molar volume in $Ia\bar{3}d$ phase for which all cations are located at special positions (Wyckoff positions: 24c, 16a, and 24d) directly reflects that of cation-cation distances.] However, both molar volume and $(O\text{-}O)_{shared}/(O\text{-}O)_{unshared}$ for each polyhedron decrease with the symmetry reduction from $Ia\bar{3}d$ to $I4_1/acd$, although the decrease in $(O\text{-}O)_{shared}/(O\text{-}O)_{unshared}$ is slight. This suggests that the crystal structure of the majorite solid-solution is energetically stabilized by the increase in the shielding effect (i.e., the decrease in the cation-cation interaction) with the symmetry reduction, and consequently the shortening of the cation-cation distances (i.e., the decrease in molar volume) is acceptable because of the decrease in the cation-cation interaction.

We can now interpret the symmetry reduction that cannot be explained by cation ordering on the octahedral sites. The site splitting due to the symmetry reduction from $Ia\bar{3}d$ to $I4_1/acd$ has the effect that one of the site symmetries of the two nonequivalent tetrahedral sites in $I4_1/acd$ structure (16e-site; site symmetry 2) loses a center of symmetry (Table 5). Furthermore, dodecahedral and tetrahedral cations deviate from the special positions in cubic symmetry ($Ia\bar{3}d$) with the symmetry reduction, although the octahedral cation maintains the special position (Table 5). On the basis of this evidence, the electronic polarization of the dodecahedral and tetrahedral cations is probably one reason for the symmetry reduction from $Ia\bar{3}d$ to $I4_1/acd$. The electronic polarization may be induced from the deformation of orbitals caused by the strong electrostatic interaction between dodecahedral and tetrahedral cations described above. Such deformation of orbitals will arise so that the increase in the shielding effect, i.e., the relative shortening of the polyhedral shared edges seen in Figure 6 is brought about with the symmetry reduction, to relax the strong cation-cation interaction. Consequently, the degree of the overlapping between the nonbonding molecular orbitals regarded as the bridge of electron density in Figure 5 will increase with the symmetry reduction from $Ia\bar{3}d$ to $I4_1/acd$ because of the relative shortening of the polyhedral shared edges; this will contribute to the energetic stabilization of the crystal structure of majorite solid-solution due to the decrease in the cation-cation interaction. Thus, the electrostatic neighboring cation-cation interaction is considered to play an important role in the symmetry reduction from $Ia\bar{3}d$ to $I4_1/acd$.

ACKNOWLEDGMENTS

This paper is a part of doctoral study of the first author submitted to the Graduate School of Science, Osaka University. A portion of this work has been done under the approval of the Photon Factory Program Advisory Committee (proposal no. 94G314).

REFERENCES CITED

Adachi, H. (1991) Introduction to Quantum Material Chemistry, p. 123–132. Sankyo Inc., Tokyo. (in Japanese)

Akaogi, M. and Akimoto, S. (1977) Pyroxene-garnet solid-solution equilibria in the system $Mg_4Si_4O_{12}$-$Mg_3Al_2Si_3O_{12}$ and $Fe_4Si_4O_{12}$-$Fe_3Al_2Si_3O_{12}$ at high pressure and temperature. Physics of Earth and Planetary Interiors, 15, 90–104.

Angel, R.J., Finger, L.W., Hazen, R.M., Kanzaki, M., Weidner, D.J., Liebermann, R.C., and Veblen, D.R. (1989) Structure and twinning of single-crystal $MgSiO_3$ garnet synthesized at 17 GPa and 1800 °C. American Mineralogist, 74, 509–512.

Brown, I.D. and Shannon, R.D. (1973) Empirical bond-strength–bond-length curves for oxides. Acta Crystallographica, A29, 266–282.

Fujino, K., Momoi, H., Sawamoto, H., and Kumazawa, M. (1986) Crystal structure and chemistry of $MnSiO_3$ tetragonal garnet. American Mineralogist, 71, 781–785.

Finger, L.W. (1969) Determination of cation distribution by least-squares refinement of single-crystal X-ray data. Carnegie Institution Year Book, 67, 216–217.

Griffen, D.T., Hatch, D.M., Phillips, W.R., and Kulaksiz, S. (1992) Crystal chemistry and symmetry of a birefringent tetragonal pyralspite$_{75}$-grandite$_{25}$ garnet. American Mineralogist, 77, 399–406.

Hatch, D.M. and Ghose, S. (1989) Symmetry analysis of the phase transition and twinning in $MgSiO_3$ garnet: Implications to mantle mineralogy. American Mineralogist, 74, 1221–1224.

Hazen, R.M., Downs, R.T., Finger, L.W., Conrad, P.G., and Gasparik, T. (1994) Crystal chemistry of Ca-bearing majorite. American Mineralogist, 79, 581–584.

Heinemann, S., Sharp, T.G., Seifert, F., and Rubie, D.C. (1997) The cubic-tetragonal phase transition in the system majorite ($Mg_4Si_4O_{12}$)-pyrope ($Mg_3Al_2Si_3O_{12}$), and garnet symmetry in the earth's transition zone. Physics and Chemistry of Minerals, 24, 206–221.

Ibers, J.A. and Hamilton, W.C., Eds. (1974) International Tables for X-ray Crystallography, vol. IV, 366 p. Kynoch, Birmingham, U.K.

Ito, E. and Takahashi, E. (1987) Ultrahigh-pressure phase transformations and the constitution of the deep mantle. In M.H. Manghnani and Y. Syono, Eds., High-pressure research in mineral physics, p. 221–230. Terra Scientific Publishing Co., Tokyo.

Johnson, C.K. (1965) ORTEP. Report ORNL-3794. Oak Ridge National Laboratory, Tennessee, U.S.A.

Kato, T. and Kumazawa, M. (1985) Garnet phase of $MgSiO_3$ filling the pyroxene-ilmenite gap at very high temperature. Nature, 316, 803–805.

Liu, L. (1977) The system enstatite-pyrope at high pressures and temperatures and the mineralogy of the earth's mantle. Earth and Planetary Science Letters, 36, 237–245.

Nakatsuka, A., Yoshiasa, A., and Takeno, S. (1995) Site preference of cations and structural variation in $Y_3Fe_{5-x}Ga_xO_{12}$ ($0 \le x \le 5$) solid solutions with garnet structure. Acta Crystallographica, B51, 737–745.

Novak, G.A. and Gibbs, G.V. (1971) The crystal chemistry of silicate garnets. American Mineralogist, 56, 791–825.

Parise, J.B., Wang, Y., Gwanmesia, G.D., Zhang, J., Sinelnikov, Y., Chmielowski, J., Weidner, D.J., and Liebermann, R.C. (1996) The symmetry of garnets on the pyrope ($Mg_3Al_2Si_3O_{12}$)-majorite ($MgSiO_3$) join. Geophysical Research Letters, 23, 3799–3802.

Ringwood, A.E. (1967) The pyroxene-garnet transformation in the earth's mantle. Earth and Planetary Science Letters, 2, 255–263.

Sawamoto, H. (1987) Phase diagram of $MgSiO_3$ at pressures up to 24 GPa and temperatures up to 2200 °C: Phase stability and properties of tetragonal garnet. In M.H. Manghnani and Y. Syono, Eds., High-pressure research in mineral physics, p. 209–219. Terra Scientific Publishing Co., Tokyo.

Shannon, R.D. (1976) Revised effective ionic radii and systematic studies of interatomic distances in halides and chalcogenides. Acta Crystallographica, A32, 751–767.

Sinogeikin, S.V., Bass, J.D., O'Neill, B., and Gasparik, T. (1997) Elasticity of tetragonal end-member majorite and solid solutions in the system $M_4Si_4O_{12}$-$Mg_3Al_2Si_3O_{12}$. Physics and Chemistry of Minerals, 24, 115–121.

Takéuchi, Y., Haga, N., Umizu, S., and Sato, G. (1982) The derivative structure of silicate garnets in grandite. Zeitschrift für Kristallographie, 158, 53–99.

Wang, Y., Gasparik, T., and Liebermann, R.C. (1993) Modulated microstructure in synthetic majorite. American Mineralogist, 78, 1165–1173.

Yoshiasa, A., Nakatsuka, A., and Ohkawa, M. (1997) EXAFS study on the short-range correlation of vibrational motion in the $Y_3Fe_{5-x}Ga_xO_{12}$ garnet solid solution. Mineralogical Journal, 19, 21–32.

MANUSCRIPT RECEIVED SEPTEMBER 23, 1997
MANUSCRIPT ACCEPTED MARCH 7, 1999
PAPER HANDLED BY GEORGE A. LAGER